

Bayesian inference via sparse Hamiltonian flows

Naitong Chen¹ Zuheng Xu¹ Trevor Campbell¹

Abstract

A Bayesian coresnet is a small, weighted subset of data that replaces the full dataset during Bayesian inference, with the goal of reducing computational cost. Although past work has shown empirically that there often *exists* a coresnet with low inferential error, efficiently constructing such a coresnet remains a challenge. Current methods tend to be slow, require a secondary inference step after coresnet construction, and do not provide bounds on the data marginal evidence. In this work, we introduce a new method—*sparse Hamiltonian flows*—that addresses all three of these challenges. The method involves first subsampling the data uniformly, and then optimizing a Hamiltonian flow parametrized by coresnet weights and including periodic *momentum quasi-refreshment steps*. Theoretical results show that the method enables an exponential compression of the dataset in a representative model, and that the quasi-refreshment steps reduce the KL divergence to the target. Real and synthetic experiments demonstrate that sparse Hamiltonian flows provide accurate posterior approximations with significantly reduced runtime compared with competing dynamical-system-based inference methods.

1. Introduction

Bayesian inference provides a coherent approach to learning from data and uncertainty assessment in a wide variety of complex statistical models. A standard methodology for performing Bayesian inference in practice is Markov chain Monte Carlo (MCMC) [Robert & Casella, 2004; Robert & Casella, 2011; Gelman et al., 2013, Ch. 11,12], which simulates a Markov chain that targets the posterior distribution. In the increasingly common setting of large-scale

data, most exact MCMC methods are intractable. This is essentially because simulating each MCMC step requires an (expensive) computation involving each data point, and many steps are required to obtain inferential results of a reasonable quality. To reduce computational cost, a typical approach is to perform the computation for a random subsample of the data, rather than the full dataset, at each step (Bardenet et al., 2017; Korattikara et al., 2014; Maclaurin & Adams, 2014; Welling & Teh, 2011; Ahn et al., 2012) (see Quiroz et al. (2018) for a recent survey). However, recent work shows that the speed benefits are outweighed by its drawbacks; uniformly subsampling at each step causes MCMC to either mix slowly or provide poor inferential approximation quality (Johnsdrow et al., 2020; Nagapetyan et al., 2017; Betancourt, 2015; Quiroz et al., 2018; 2019).

Another methodology for Bayesian inference is variational inference (VI) (Jordan et al., 1999; Wainwright & Jordan, 2008), which posits a family of approximations to the posterior and optimizes an objective to find the closest member. VI, in contrast to MCMC, is tractable in the large-scale data setting: one can use stochastic gradient estimates (Hoffmann et al., 2013; Ranganath et al., 2014) based on subsampling to reduce computational cost. A major drawback of VI, however, is that parametric distribution families are limited and do not generally enable arbitrarily accurate posterior approximation. An exciting line of recent work in VI has started to tackle this problem by constructing VI families from parametrized Markov chains (Salimans et al., 2015; Habib & Barber, 2018)—and in particular, those based on Langevin and Hamiltonian dynamics (Wolf et al., 2016; Caterini et al., 2018; Neal, 2005; Geffner & Domke, 2021; Zhang et al., 2021a; Thin et al., 2021). However, because these Markov chains are typically designed to target the posterior of interest, KL minimization and sampling are both slow in the large-data regime; and repeated subsampling to reduce cost has the same issues that it does in MCMC.

Although subsampling the data in each step of MCMC or a variational flow is not generally helpful, the notion of working with a subset of data rather than the full dataset is still reasonable. In many problems, we expect redundancy in the data that should, in principle, mean that we do not require the entire dataset for inference. Indeed, recent work on *Bayesian coresets* (Huggins et al., 2016)—inspired by the coresets literature from computational geometry (Agarwal

¹Department of Statistics, University of British Columbia, Vancouver, Canada. Correspondence to: Naitong Chen <naitong.chen@stat.ubc.ca>, Zuheng Xu <zuheng.xu@stat.ubc.ca>, Trevor Campbell <trevor@stat.ubc.ca>.

et al., 2005) and optimization (Feldman & Langberg, 2011; Feldman et al., 2011; 2013)—has provided empirical evidence that there often *exists* a fixed, weighted subset of the data (a *coreset*) that one can use to replace the full dataset in a standard MCMC or VI inference method (Campbell & Beronov, 2019). In order for the Bayesian coresets approach to be practically useful, one must (1) find a suitable sparse, weighted subset of data that provides a good posterior approximation; and (2) do so quickly enough that the speed-up of inference is worth the time it takes to find the coresets, including tuning effort. There is currently no option that satisfies these two desiderata. Importance weighting methods (Huggins et al., 2016) are fast, but do not provide adequate approximations in practice. Sparse linear regression methods (Campbell & Broderick, 2019; 2018; Zhang et al., 2021b) are fast and potentially provide high-quality approximations, but are very difficult to tune well. And sparse variational methods (Campbell & Beronov, 2019; Manousakas et al., 2020) find very high quality coresets approximations without undue tuning effort, but are too slow to be practical.

This work introduces three key insights. First, we can uniformly subsample the dataset once to pick the points in the coresets (the weights still need to be optimized). This selection is not only significantly simpler than past algorithms; we show that it enables constructing an *exact* coresets—with KL divergence 0 to the posterior—of size $O(\log_2(N))$ for N data points in a representative model (Proposition 3.1). Second, we can then construct a normalizing flow family based on Hamiltonian dynamics (Rezende & Mohamed, 2015; Caterini et al., 2018; Neal, 2005) that targets the coresets posterior (parametrized by coresets weights) rather than the expensive full posterior. This method address all of the current challenges with coresets: it enables tractable i.i.d. sampling, provides a known density and normalization constant (and hence marginal evidence lower bound), and is tuned using straightforward KL minimization with stochastic gradients. It also addresses the inefficiency of Markov-chain-based VI families, as the Markov chain steps are computed using the inexpensive coresets posterior density rather than the full posterior density¹. The final insight is that past momentum tempering methods (Caterini et al., 2018) do not provide sufficient flexibility for arbitrary approximation to the posterior, even in a simple setting (Proposition 3.2). Thus, we introduce novel periodic *momentum quasi-refreshment* steps that provably reduce the KL objective (Propositions 3.3 and 3.4). The paper concludes with real and synthetic experiments, demonstrating

¹The use of a weighted subsample of data to construct a Hamiltonian flow-based posterior approximation was also developed in concurrent work in the context of variational annealed importance sampling (Jankowiak & Phan, 2021); our work focuses on normalizing flows.

that sparse Hamiltonian flows compare favourably to both current coresets compression methods and variational flow-based families. Proofs of all theoretical results may be found in the appendix.

2. Background

2.1. Bayesian Coresets

We are given a target probability density $\pi(\theta)$ for variables $\theta \in \mathbb{R}^d$ that takes the following form:

$$\pi(\theta) = \frac{1}{Z} \exp \left(\sum_{n=1}^N f_n(\theta) \right) \pi_0(\theta).$$

In a Bayesian inference problem with i.i.d. data, π_0 is the prior density, the f_n are the log-likelihood terms for N data points, and the normalization constant is in general not known. The goal is to take samples from the distribution corresponding to density $\pi(\theta)$.

In order to avoid the $\Theta(N)$ cost of evaluating $\log \pi(\theta)$ or $\nabla \log \pi(\theta)$ (at least one of which must be conducted numerous times in most standard inference algorithms), *Bayesian coresets* (Huggins et al., 2016) involve replacing the target with a surrogate density of the form

$$\pi_w(\theta) = \frac{1}{Z(w)} \exp \left(\sum_{n=1}^N w_n f_n(\theta) \right) \pi_0(\theta),$$

where $w \in \mathbb{R}^N$, $w \geq 0$ are a set of nonnegative weights. Assuming the weights have at most $M \ll N$ nonzero entries, the $O(M)$ cost of evaluating $\log \pi_w(\theta)$ or $\nabla \log \pi_w(\theta)$ is a significant improvement upon the original $\Theta(N)$ cost.

2.2. Bayesian Coreset Construction

The baseline method to construct a coresets is to draw a uniformly random subsample of M data points, and give each a weight of N/M ; although this method is quite fast in practice, it typically generates poor posterior approximations. One can also draw the subsample from a nonuniform distribution and set the weights via an importance sampling scheme, but these methods typically provide little practical improvement over the uniformly random baseline (Huggins et al., 2016). A second class of methods involve building the coresets using sparse optimization, adding one data point at a time to the coresets and then tuning the weights. Campbell & Broderick (2019; 2018); Zhang et al. (2021b) formulate a sparse linear regression problem in a weighted L^2 space,

$$w^* = \arg \min_{w \in \mathbb{R}_+^N} \left\| \sum_{n=1}^N g_n - \sum_{n=1}^N w_n g_n \right\|_{L^2(\hat{\pi})}^2 \quad \text{s.t.} \quad \|w\|_0 \leq M,$$

where $g_n(\theta) = f_n(\theta) - \mathbb{E}_{\hat{\pi}} f_n(\theta)$; but this method requires the user to specify the weighting function $\hat{\pi}$, which is not

straightforward in practice. Campbell & Beronov (2019); Manousakas et al. (2020) instead formulate the problem as variational inference and provide a stochastic gradient scheme using samples from π_w ,

$$w^* = \arg \min_{w \in \mathbb{R}_+^N} D_{\text{KL}}(\pi_w || \pi) \quad \text{s.t.} \quad \|w\|_0 \leq M.$$

Empirically, this method tends to produce very high-quality coresets (Campbell & Beronov, 2019). However, estimating the gradients requires that one samples from the coreset posterior. While theoretically not expensive, interleaving MCMC and gradient descent steps is hard to implement and tune, and is too slow to be practical. Once the coreset is constructed, all of the aforementioned methods requires a secondary inference algorithm to take draws from π_w . Further, since $Z(w)$ is not known in general, it is not tractable to use these methods to bound the marginal evidence Z .

2.3. Hamiltonian Dynamics

In this section we provide a very brief overview of some important aspects of a special case of Hamiltonian dynamics and its use in statistics; see Neal (2011) for a more comprehensive overview. Let $U \in \mathbb{R}^{d \times d}$ be a symmetric positive definite matrix. The differential equation below in Eq. (1) describes how a (deterministic) Hamiltonian system with position $\theta_t \in \mathbb{R}^d$, momentum $\rho_t \in \mathbb{R}^d$, differentiable negative potential energy $\log \pi(\theta_t)$, and kinetic energy $\frac{1}{2} \rho_t^T U \rho_t$ evolves over time $t \in \mathbb{R}$:

$$\frac{d\rho_t}{dt} = \nabla \log \pi(\theta_t) \quad \frac{d\theta_t}{dt} = U \rho_t. \quad (1)$$

For $t \in \mathbb{R}$, define the mappings $H_t : \mathbb{R}^{2d} \rightarrow \mathbb{R}^{2d}$ that take $(\theta_s, \rho_s) \mapsto (\theta_{s+t}, \rho_{s+t})$ under the dynamics in Eq. (1). These mappings have two key properties that make Hamiltonian dynamics useful in statistics. First, they are invertible, and preserve volume in the sense that $|\det \nabla H_t| = 1$. In other words, they provide tractable density transformations: for any density q on \mathbb{R}^{2d} and pushforward q_t on \mathbb{R}^{2d} under the mapping H_t ,

$$\forall t \in \mathbb{R}, \quad q_t(\cdot, \cdot) = q(H_t^{-1}(\cdot, \cdot)). \quad (2)$$

Second, the *augmented target density* $\bar{\pi}(\theta, \rho)$ on \mathbb{R}^{2d} ,

$$\bar{\pi}(\theta, \rho) \propto \pi(\theta) \cdot \exp\left(-\frac{1}{2} \rho^T U \rho\right),$$

(i.e., the density of the distribution of independent draws from π and $\mathcal{N}(0, U^{-1})$) is invariant under the mappings H_t :

$$\forall t \in \mathbb{R}, \quad \bar{\pi}(H_t(\cdot, \cdot)) = \bar{\pi}(\cdot, \cdot). \quad (3)$$

Given these properties, Hamiltonian Monte Carlo (Neal, 2011; 1996) constructs a Gibbs sampler for $\bar{\pi}$ that interleaves Hamiltonian dynamics—to sample within level sets

of total energy—with periodic stochastic momentum refreshments $\rho \sim \mathcal{N}(0, U^{-1})$ that mix over energy levels. Upon completion, the ρ component of the samples can be dropped to obtain samples from the desired target π .

In practice, one approximately simulates the dynamics in Eq. (1) using the leapfrog method, which involves interleaving three discrete transformations with step size $\epsilon > 0$,

$$\begin{aligned} \hat{\rho}_{k+1} &= \rho_k + \frac{\epsilon}{2} \nabla \log \pi(\theta_k) \\ \theta_{k+1} &= \theta_k + \epsilon U \hat{\rho}_{k+1} \\ \rho_{k+1} &= \hat{\rho}_{k+1} + \frac{\epsilon}{2} \nabla \log \pi(\theta_{k+1}) \end{aligned} \quad (4)$$

Denote the map constructed by applying these three steps in sequence $T_\epsilon : \mathbb{R}^{2d} \rightarrow \mathbb{R}^{2d}$. As the transformations in Eq. (4) are all shear, T_ϵ is also volume-preserving, and for small enough step size ϵ it nearly maintains the target invariance. Note also that evaluating a single application of T_ϵ is of $O(Nd)$ complexity, which is generally expensive in the large-data (large- N) regime.

2.4. VI via Hamiltonian Dynamics

Since the mapping T_ϵ is invertible and volume-preserving, it is possible to tractably compute the density of the push-forward of a reference distribution $q(\cdot, \cdot)$ under repeated applications of it. Caterini et al. (2018); Neal (2005) use this fact to construct a normalizing flow (Rezende & Mohamed, 2015) VI family. However, there are two issues with this methodology. First, the $O(Nd)$ complexity of evaluating each step T_ϵ makes training and simulating from this flow computationally expensive. Second, Hamiltonian dynamics on its own creates a flow with insufficient flexibility to match a target $\bar{\pi}$ of interest. In particular, Eqs. (2) and (3) together imply that if we are given a density $q(\cdot, \cdot)$ and pushforward $q_t(\cdot, \cdot)$ under H_t , then

$$\forall t \in \mathbb{R}, \quad D_{\text{KL}}(q_t || \bar{\pi}) = D_{\text{KL}}(q || \bar{\pi}).$$

In other words, the Hamiltonian dynamics itself cannot reduce the KL divergence to $\bar{\pi}$; it simply interchanges potential and kinetic energy. Caterini et al. (2018) address this issue by instead deriving their flow from *tempered* Hamiltonian dynamics: for an integrable tempering function $\gamma : \mathbb{R} \rightarrow \mathbb{R}$,

$$\frac{d\rho_t}{dt} = \nabla \log \pi(\theta_t) - \gamma(t) \rho_t \quad \frac{d\theta_t}{dt} = U \rho_t. \quad (5)$$

The discretized version of the dynamics in Eq. (5) corresponds to multiplying the momentum by a tempering value $\alpha_k > 0$ after the k^{th} application of T_ϵ . By scaling the momentum, one provides the normalizing flow with the flexibility to change the kinetic energy at each step. However, we show later in Proposition 3.2 that just tempering the

momentum does not provide the required flow flexibility, even in a simple representative model Eq. (6).

A related line of work uses the mapping T_ϵ for variational annealed importance sampling (Geffner & Domke, 2021; Zhang et al., 2021a; Thin et al., 2021). The major difference between these methods and the normalizing flow-based methods is that the auxiliary variable is (partially) stochastically refreshed via $\rho \sim \mathcal{N}(0, U^{-1})$ after applications of T_ϵ . One is then forced to minimize the KL divergence between the joint distribution of θ and all of the auxiliary momentum variables under the variational and augmented target distributions.

3. Sparse Hamiltonian flows

In this section we present sparse Hamiltonian flows, a new method to construct and draw samples from Bayesian coresets posterior approximations. We first present a method and supporting theory for selecting the data points to be included in the coreset, then discuss building a sparse flow with these points, and finally introduce quasi-refreshment steps to give the flow family enough flexibility to match the target distribution. Sparse Hamiltonian flows enables tractable i.i.d. sampling, provides a tractable density and normalization constant, and is constructed by minimizing the KL divergence to the posterior with simple stochastic gradient estimates.

Throughout, we will use the following simple Bayesian Gaussian location model—a representative model for many log-concave families—to motivate the developments and obtain theoretical insight into our method:

$$\theta \sim \mathcal{N}(0, I) \quad \text{and} \quad \forall n \in [N], \quad X_n \stackrel{\text{i.i.d.}}{\sim} \mathcal{N}(\theta, I), \quad (6)$$

where $\theta, X_n \in \mathbb{R}^d$ for $d \in \mathbb{N}$. This model has closed-form posterior π and coreset posterior π_w given by

$$\begin{aligned} \pi &= \mathcal{N}\left(\frac{\sum_{n=1}^N X_n}{1+N}, \frac{1}{1+N}I\right) \\ \pi_w &= \mathcal{N}\left(\frac{\sum_{n=1}^N w_n X_n}{1+\sum_n w_n}, \frac{1}{1+\sum_n w_n}I\right). \end{aligned}$$

3.1. Selection via subsampling

The first step in our algorithm is to choose a uniformly random subsample of M points from the full dataset; these will be the data points that comprise the coreset. The key insight in this work is that while subsampling (and subsequent importance weighting) does not typically provide good coresset approximations (Huggins et al., 2016), a uniformly random subset of the N log-likelihood potential functions $\{f_1, \dots, f_M\}$ still provides a good *basis* for approximation (w.l.o.g., we can assume these are the first M

potentials) with high probability. Proposition 3.1 provides the precise statement of this result for the running example model Eq. (6). In particular, Proposition 3.1 asserts that as long as we set our coreset size M to be proportional to $d \log_2 N$, the optimal coreset posterior approximation will be *exact*, i.e., have 0 KL divergence to the true posterior, with probability at least $1 - N^{-\frac{d}{2}}(\log_2 N)^{\frac{d}{2}}$. Thus we achieve an exponential compression of the dataset, $N \rightarrow \log_2 N$, without losing any fidelity. Note that we will still need a method to choose the weights w_1, \dots, w_M for the M points, but the use of uniform selection rather than the one-at-a-time approach of previous methods (Campbell & Broderick, 2018; 2019; Campbell & Beronov, 2019) substantially simplifies the construction. In Proposition 3.1, let C be the universal constant from Böröczky & Wintzsche (2003, Corollary 1.2).

Proposition 3.1. *Suppose $(X_n)_{n=1}^N \stackrel{\text{i.i.d.}}{\sim} \mathcal{N}(0, I)$, and set*

$$M = \log_2(A_d N^d (\log N)^{-d/2}) + C$$

$$\text{where } A_d = e^{\frac{d}{2}} d^{\frac{3}{2}} \log(1+d).$$

Then the optimal coreset π_{w^} for the model Eq. (6) built using a uniform subsample of data of size M satisfies*

$$\limsup_{N \rightarrow \infty} \frac{\mathbb{P}(\text{D}_{\text{KL}}(\pi_{w^*} \parallel \pi) \neq 0)}{N^{-\frac{d}{2}} (\log N)^{\frac{d}{2}}} \leq 1.$$

3.2. Sparse flows

Upon taking a uniform subsample of M data points from the full dataset, we consider the sparsified Hamiltonian dynamics initialized at $\theta_0, \rho_0 \sim q(\cdot, \cdot)$ for $q(\cdot, \cdot)$ a reference density²

$$\frac{d\rho_t}{dt} = \nabla \log \pi_w(\theta_t) \quad \frac{d\theta_t}{dt} = U\rho_t, \quad (7)$$

where for simplicity we assume we rearrange the indices so that the subsample corresponds to the first M indices, i.e., $w_n = 0$ for $n > M$. Much like the original Hamiltonian dynamics for the full target density, the sparsified Hamiltonian dynamics Eq. (7) targets the augmented coreset posterior with density $\bar{\pi}_w(\theta, \rho)$ on \mathbb{R}^{2d} ,

$$\bar{\pi}_w(\theta, \rho) \propto \pi_w(\theta) \exp\left(-\frac{1}{2}\rho^T U \rho\right).$$

Discretizing these dynamics yields a leapfrog method similar to Eq. (4) that involves three interleaved steps,

$$\begin{aligned} \hat{\rho}_{k+1} &= \rho_k + \frac{\epsilon}{2} \nabla \log \pi_w(\theta_k) \\ \theta_{k+1} &= \theta_k + \epsilon U \hat{\rho}_{k+1} \\ \rho_{k+1} &= \hat{\rho}_{k+1} + \frac{\epsilon}{2} \nabla \log \pi_w(\theta_{k+1}) \end{aligned} \quad . \quad (8)$$

²The reference q can also have its own variational parameters to optimize, but in this paper we leave it fixed for simplicity.

Denote the map constructed by applying these three steps in sequence $T_{w,\epsilon} : \mathbb{R}^{2d} \rightarrow \mathbb{R}^{2d}$. Like the original leapfrog method, these transformations are both invertible and shear, and thus preserve volume; and for small enough step size ϵ , they approximately maintain the invariance of $\bar{\pi}_w(\theta, \rho)$. However, since w only has the first M entries nonzero,

$$\nabla \log \pi_w(\theta_k) = \sum_{m=1}^M w_m \nabla \log f_m(\theta_k),$$

and thus a coresnet leapfrog step can be taken in $O(Md)$ time, as opposed to $O(Nd)$ time in the original approach. Given that Proposition 3.1 recommends setting $M \approx d \log_2(N)$, we have achieved an exponential reduction in computational cost of running the flow.

However, as before, the weighted sparse leapfrog flow is not sufficient on its own to provide a flexible variational family. In particular, we know that $T_{w,\epsilon}$ nearly maintains the distribution $\bar{\pi}_w$ as invariant. We therefore need a way to modify the distribution of the momentum variable ρ . One option is to include a tempering of the form Eq. (5) into the sparse flow. However, Proposition 3.2 demonstrates that this does not add sufficient flexibility, even in the simple running example model Eq. (6); the *optimal* tempering still does not provide the ability to match the true augmented target $\bar{\pi}$, even in the simple model Eq. (6).

Proposition 3.2. *Let $\theta_t, \rho_t \in \mathbb{R}$ follow the tempered Hamiltonian dynamics Eq. (5) with $U = 1$ targeting $\pi = \mathcal{N}(0, \sigma^2)$, $\sigma > 0$, with initial distribution $\theta_0 \sim \mathcal{N}(\mu, 1)$, $\rho_0 \sim \mathcal{N}(0, \beta^2)$ for initial center $\mu \in \mathbb{R}$ and momentum scale $\beta > 0$. Let q_t be the distribution of (θ_t, ρ_t) . Then*

$$\inf_{t>0, \beta>0, \gamma: \mathbb{R}_+ \rightarrow \mathbb{R}} D_{\text{KL}}(q_t \parallel \bar{\pi}) \geq \log \frac{1 + \mu^2}{4\sigma}.$$

Note that if $\gamma(t) = 0$ identically,

$$\forall t \geq 0, \quad D_{\text{KL}}(q_t \parallel \bar{\pi}) = D_{\text{KL}}(q_0 \parallel \bar{\pi}).$$

The intuition behind Proposition 3.2 is that while adding a tempering $\gamma(t)$ enables one to increase or decrease the total energy in the system by scaling the momentum, it does not allow one fine enough control on the distribution of the momentum. For example, in the setting of Proposition 3.2, we would ideally like to make a change to the momentum distribution roughly when the flow reaches the θ -mode of $\bar{\pi}$ at $\theta = 0$ (where the marginal distribution of θ will roughly match π). But if the θ marginal of the initial distribution is centered far from the mode (say, μ is large and positive), when the flow reaches this θ -mode, the momentum distribution will be concentrated largely on a value pointing in the negative direction. Scaling the momentum at this point will not help; intuitively, we also need the ability to shift or recenter the momentum at this point, not just scale it.

Hamiltonian Monte Carlo (Neal, 2011) achieves this by refreshing the momentum ρ_t from its target marginal distribution $\mathcal{N}(0, U^{-1})$; but this removes the ability to efficiently calculate the density and normalization constant of θ_t, ρ_t .

3.3. Quasi-refreshment

Rather than resampling the momentum variable from its target marginal—which removes the ability to evaluate the density of θ_t, ρ_t —in this work we introduce deterministic *quasi-refreshment* moves that enable the flow to strategically update the momentum without losing the ability to compute the density and normalization constant of θ_t, ρ_t (i.e., we construct a normalizing flow (Rezende & Mohamed, 2015)). In this section, we introduce two kinds of quasi-refreshment—marginal and conditional—which aim to manipulate carefully-chosen marginal or conditional distributions of (θ_t, ρ_t) to match the corresponding marginal or conditional distribution of the augmented coresnet target $\bar{\pi}_w$. For clarity, we will assume $U = I$ from this point onward in the paper.³

Marginal quasi-refreshment The first (and simplest) kind of quasi-refreshment move is one that tries to make a marginal distribution of ρ_t match the corresponding marginal distribution of the augmented target $\bar{\pi}_w$. Proposition 3.3 shows that as long as the corresponding marginal in the augmented target is independent of the other variables, this type of move is guaranteed to reduce the KL divergence (by an amount corresponding to the selected marginal KL divergence).

Proposition 3.3. *Consider random vectors $X, W, Y, Z \in \mathbb{R}^d$ for some $d \in \mathbb{N}$. Suppose that $Y \perp\!\!\!\perp Z$ and that we have a bijection $R : \mathbb{R}^d \rightarrow \mathbb{R}^d$ such that $R(X) \stackrel{d}{=} Y$. Then*

$$D_{\text{KL}}(R(X), W \parallel Y, Z) = D_{\text{KL}}(X, W \parallel Y, Z) - D_{\text{KL}}(X \parallel Y).$$

In order to apply Proposition 3.3, we first need to split the momentum variable into two components $(\rho^{(1)}, \rho^{(2)})$ in such a way that $\rho^{(1)} \perp\!\!\!\perp \rho^{(2)}$ under $(\theta, \rho) \sim \bar{\pi}$, and then set $Y = \rho^{(1)}$ and $Z = (\rho^{(2)}, \theta)$. Since we know that $\rho \sim \mathcal{N}(0, I)$, we have quite a few options. For example:

- Set $Y = \rho$, and $Z = \theta$. Then

$$Y \perp\!\!\!\perp Z \quad \text{and} \quad Y \sim \mathcal{N}(0, I).$$

- Set $Y = \|D\rho\|_2^2$ and $Z = \left(\frac{D\rho}{\|D\rho\|_2^2}, (I - D)\rho, \theta \right)$ for any binary diagonal matrix $D \in \mathbb{R}^{d \times d}$. Then

$$Y \perp\!\!\!\perp Z \quad \text{and} \quad Y \sim \chi^2(\text{tr } D).$$

³The marginal and conditional quasi-refresh steps can be easily modified for general U by taking the Cholesky decomposition $U = LL^T$, transforming $\rho \leftarrow L^T \rho$ prior to refreshment, and then reverse transforming $\rho \leftarrow L^{-T} \rho$ afterward.

- Set $Y = a^T \rho$ for any $a \in \mathbb{R}^d$ such that $\|a\| = 1$, and $Z = ((I - aa^T)\rho, \theta)$. Then

$$Y \perp\!\!\!\perp Z \quad \text{and} \quad Y \sim \mathcal{N}(0, 1).$$

Now we use the above decomposition to design a marginal quasi-refreshment move. Suppose we have run the weighted sparse leapfrog integrator Eq. (8) up to time t , resulting in a current random state θ_t, ρ_t . Let the decomposition of the current state (θ_t, ρ_t) that we select above be denoted Y_t, Z_t . Then the marginal quasi-refreshment move involves finding a map R such that $R(Y_t) \stackrel{d}{=} Y$. We can then refresh the state via $(R(Y_t), Z_t)$, and continue the flow. There are generally two approaches to obtaining an appropriate map R . First, if we are willing to make an assumption about the distribution of the momentum, we can introduce a tunable family of functions R_λ with parameters λ , and include optimization of λ along with the coresets weights. For example, if we assume that $\rho_t \sim \mathcal{N}(\mu, \Lambda^{-1})$ for some unknown mean μ and diagonal precision Λ , then we can take the simple approach of setting $Y_t = \rho_t$ and

$$R(x) = \Lambda(x - \mu), \quad (9)$$

and then include Λ and μ as parameters to be optimized along with the coresets weights w . Although this approach requires making an assumption about the distribution of ρ_t , the resulting form of Eq. (9) enables the refreshment step to both shift and scale (i.e., standardize) the momentum, as required. Second, if Y is 1-dimensional—for example, if we are trying to refresh the momentum norm $Y = \|\rho\|_2$ —then given that we know the CDF F of Y , we can estimate the CDF \hat{F} of Y_t using samples from the flow at timestep t , and then set

$$R(x) = F^{-1}(\hat{F}(x)).$$

For example, we could use this inverse CDF map technique to refresh the distribution of $\|\rho\|_2^2$ back to $\chi^2(d)$, or to refresh the distribution of $a^T \rho$ back to $\mathcal{N}(0, 1)$.

In our experiments we take the first approach, as it is easier to implement as part of a single optimization routine. Fig. 1 provides an example of the effect of quasi-refreshment in a simple synthetic Gaussian location model (see Section 4.1 for details). In particular, it shows the evidence lower bound (ELBO) as a function of leapfrog step number in a trained sparse Hamiltonian flow with the marginal standardization quasi-refreshment scheme in Eq. (9). Quasi-refreshment steps are colored red. While the estimated ELBO values stay relatively stable across leapfrog steps in between quasi-refreshments, the quasi-refreshment steps cause the ELBO to increase drastically. As the series of transformations brings the approximated density closer to the target, the quasi-refreshment steps no longer change

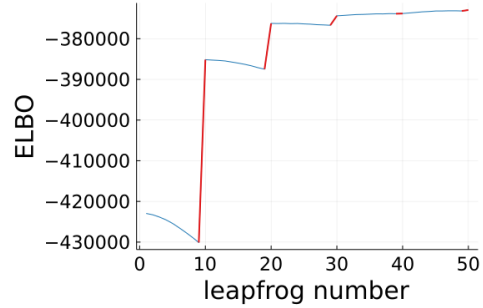


Figure 1. Evolution of ELBO across leapfrog steps.

the ELBO much, signalling the convergence of the flow’s approximation of the target. It is thus clear that the marginal quasi-refreshments indeed decrease the KL, as shown in Proposition 3.3.

Conditional quasi-refreshment A conditional quasi-refreshment move is one that tries to make some conditional distribution of (ρ_t, θ_t) match the same conditional in the target. If one is able to accomplish this for *any* conditional distribution (with no requirement of independence as in the marginal case), the KL divergence is guaranteed to reduce.

Proposition 3.4. *Consider random vectors $X, W, Y, Z \in \mathbb{R}^d$ for some $d \in \mathbb{N}$. Suppose for each $s \in \mathbb{R}^d$ we have a bijection $R_s : \mathbb{R}^d \rightarrow \mathbb{R}^d$ such that $(R_s(X) \mid W = s) \stackrel{d}{=} (Y \mid Z = s)$. Then*

$$\text{D}_{\text{KL}}(R_W(X), W \mid\mid Y, Z) = \text{D}_{\text{KL}}(W \mid\mid Z).$$

Conditional moves are much harder to design than marginal moves in general. One case of particular utility occurs when one is willing to assume that (θ_t, ρ_t) are roughly jointly normally distributed. In this case,

$$\begin{pmatrix} \theta_t \\ \rho_t \end{pmatrix} \sim \mathcal{N} \left(\begin{pmatrix} \mu_\theta \\ \mu_\rho \end{pmatrix}, \begin{pmatrix} \Sigma_{\theta\theta} & \Sigma_{\theta\rho} \\ \Sigma_{\theta\rho}^T & \Sigma_{\rho\rho} \end{pmatrix} \right),$$

so one can refresh the momentum ρ_t by updating it to $R_{\theta_t}(\rho_t)$, where

$$\begin{aligned} R_s(x) &= \Sigma^{-1/2} (x - \mu_\rho - \Sigma_{\theta\rho}^T \Sigma_{\theta\theta}^{-1} (s - \mu_\theta)) \\ &= \Sigma_{\rho\rho} - \Sigma_{\theta\rho}^T \Sigma_{\theta\theta}^{-1} \Sigma_{\theta\rho}. \end{aligned}$$

In order to use this quasi-refreshment move, one can either include the covariance matrices and mean vectors as tunable parameters in the optimization, or use samples from the flow at step t to estimate them directly.

3.4. Algorithm

In this section, we describe the procedure for training and generating samples from a sparse Hamiltonian flow. As a

normalizing flow, a sparse Hamiltonian flow can be trained by maximizing the augmented ELBO of position and momentum using usual stochastic gradient methods (see, e.g., [Rezende & Mohamed \(2015\)](#)), where the transformations follow Eq. (8) with a periodic quasi-refreshment of choice. Here and in the experiments we focus on the parametrized marginal quasi-refreshment based on normal standardization in Eq. (9), but the techniques here can be generalized to other quasi-refreshment steps.

We begin by selecting a subset of M log-likelihood potential functions chosen uniformly randomly from the full set of N , which serves as our coresnet basis. Next we select a total number R of quasi-refreshment steps, and a number L of leapfrog steps to take between each quasi-refreshment (resulting in $L \times R$ total leapfrogs). We set $U = I$. The flow parameters to be optimized consist of the quasi-refreshment parameters $\lambda = (\lambda_r)_{r=1}^R$, a set of nonnegative M coresnet weights $w = (w_m)_{m=1}^M$, and a set of leapfrog step sizes $\epsilon = (\epsilon_i)_{i=1}^d$; note that we modify the Hamiltonian flow to have a separate step size ϵ_i per latent variable dimension i , and modify the coresnet leapfrog map $T_{w,\epsilon}$ in Eq. (8) accordingly ([Neal, 2011](#), Sec. 4.2). This modification gives the flow additional flexibility to fit nonisotropic target distributions.

We initialize the weights to N/M (i.e., a uniform coresnet), and select an initial step size for all dimensions. We use a warm start to initialize the parameters $\lambda_r = (\mu_r, \Lambda_r)$ of the quasi-refreshments. Specifically, using the initial leapfrog step sizes and coresnet weights, we pass a batch of samples from the reference density $q(\cdot, \cdot)$ through the flow up to the first quasi-refreshment step. We initialize μ_1, Λ_1 to the empirical mean and diagonal precision of the samples at that point. We then apply the initialized first quasi-refreshment to the momentum, and proceed with the second sequence of L leapfrog steps, initialize μ_2, Λ_2 to the empirical mean and precision, apply the initialized second quasi-refreshment, and repeat until we have initialized all quasi-refreshments $r = 1, \dots, R$.

Once the parameters are initialized, we log-transform the step sizes, weights, and quasi-refreshment diagonal scaling matrices to make them unconstrained during optimization. We obtain an unbiased estimate of the augmented ELBO gradient by applying automatic differentiation ([Baydin et al., 2018](#); [Kucukelbir et al., 2017](#)) to the ELBO estimation function Algorithm 2, and optimize all parameters jointly using a gradient-based stochastic optimization technique such as SGD ([Robbins & Monro, 1951](#); [Bottou, 2004](#)) and ADAM ([Kingma & Ba, 2014](#)). Once trained, we can easily obtain samples from the approximated target by extracting θ from the output of Algorithm 1.

Algorithm 1 SparseHamFlow

Require: $\theta_0, \rho_0, w, \epsilon, \lambda, L, R$
 $J \leftarrow 0$, and $(\theta, \rho) \leftarrow (\theta_0, \rho_0)$
for $r = 1, \dots, R$ **do**
 for $\ell = 1, \dots, L$ **do**
 Sparse flow leapfrog:
 $\theta, \rho \leftarrow T_{w,\epsilon}(\theta, \rho)$
 end for
 Accumulate log Jacobian determinant:
 $J \leftarrow J + \log |\det \frac{\partial R_{\lambda_r}}{\partial \rho}(\rho, \theta)|$
 Quasi-refreshment:
 $\rho \leftarrow R_{\lambda_r}(\rho, \theta)$
end for
return θ, ρ, J

Algorithm 2 Estimate_ELBO

Require: $q, \pi_0, w, \epsilon, \lambda, L, R, S$
 $(\theta_0, \rho_0) \sim q(\cdot, \cdot)$
Forward pass:
 $\theta, \rho, J \leftarrow \text{SparseHamFlow}(\theta_0, \rho_0, w, \epsilon, \lambda, L, R)$
Obtain unbiased ELBO estimate:
 $(n_1, \dots, n_S) \stackrel{\text{i.i.d.}}{\sim} \text{Unif}(\{1, 2, \dots, N\})$
 $\log \bar{p} \leftarrow \log \pi_0(\theta) + \frac{N}{S} \sum_{s=1}^S f_{n_s}(\theta) + \log \mathcal{N}(\rho \mid 0, I)$
 $\log \bar{q} \leftarrow q(\theta_0, \rho_0) - J$
return $\log \bar{p} - \log \bar{q}$

4. Experiments

In this section, we compare the quality of posterior approximation, as well as the training and sampling times of sparse Hamiltonian flows (SHF), Hamiltonian importance sampling (HIS) ([Caterini et al., 2018](#)), and unadjusted Hamiltonian annealing(UHA) ([Geffner & Domke, 2021](#)) using real and synthetic datasets. We also include sampling times of adaptive HMC and NUTS ([Hoffman & Gelman, 2014](#), Alg. 5 and 6) using the full dataset. Finally, we compare the quality of coressets constructed by SHF to those obtained using uniform subsampling (UNI) and Hilbert coresets constructed using orthogonal matching pursuit (Hilbert-OMP) ([Campbell & Broderick, 2019](#); [Pati et al., 1993](#)). In all experiments, SHF uses the shift-and-scale marginal quasi-refreshment from Eq. (9); $(\mu_r, \Lambda_r)_{r=1}^R$ are initialized using the warm-start procedure in Section 3 with a batch of 100 samples. All evaluation metrics are estimated using 100 samples. Experiments were performed on a machine with an AMD Ryzen9 3900X processor and 32GB memory. Details of the experiments may be found in Appendix A.

Note that we were unable to train HIS/UHA with full-dataset flow dynamics; even on a small 2-dimensional Gaussian location model with 100 data points, these methods took over 8 minutes for training. Therefore, as sug-

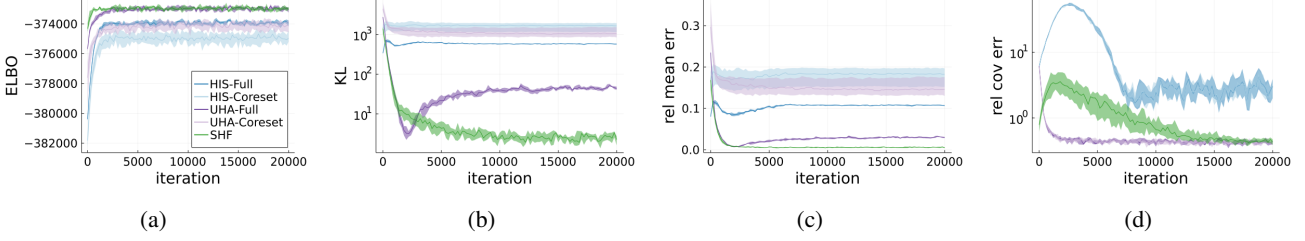


Figure 2. Comparison of performance metrics for the synthetic Gaussian problem: ELBO (Fig. 2a), KL divergence (Fig. 2b), relative 2-norm mean error (Fig. 2c), and relative Frobenius norm covariance error (Fig. 2d).

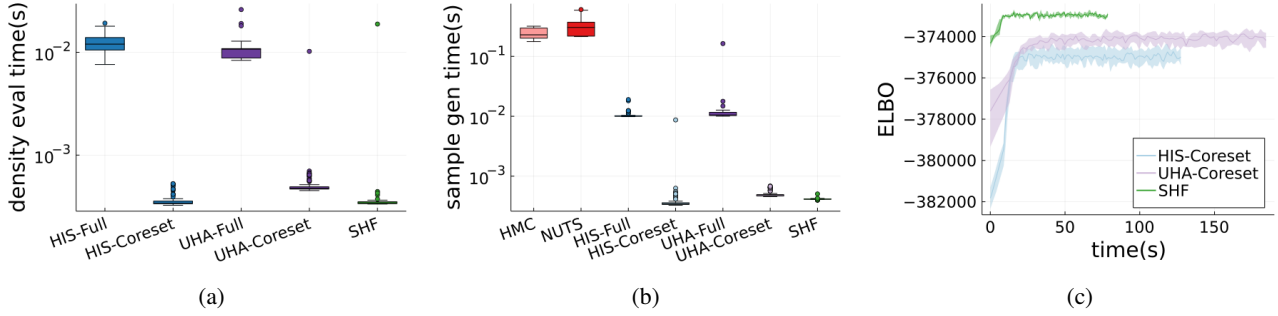


Figure 3. Comparison of timing results for the synthetic Gaussian problem: density evaluation time (Fig. 3a), sample generation time (Fig. 3b), and ELBO versus time during training (Fig. 3c).

gested by Caterini et al. (2018); Geffner & Domke (2021), we train the leapfrog step sizes and annealing parameters by using a random minibatch of the data in each iteration to construct the flow dynamics. To then obtain valid ELBO estimates for comparison, we generate samples from the trained flow with leapfrog transformations based on the full dataset (HIS-Full/UHA-Full). As a simple heuristic baseline that also provides a valid ELBO estimate, we compare to the trained flow with leapfrog transformations based on a fixed, uniformly sampled coresset (HIS-Coreset/UHA-Coreset) of the same size as used for SHF (set to 30 for all experiments). We use the same number of leapfrog, tempering, and (quasi-)refreshment steps for all of SHF, HIS and UHA respectively. The leapfrog step sizes are initialized at the same value for all three methods. We tune adaptive HMC and NUTS with a target acceptance rate of 0.65 during a number of burn-in iterations equal to the number of output samples, and include the burn-in time in the timing results for these two methods. For Hilbert-OMP, we use a random log-likelihood function projection of dimension $50d$, where the true posterior parameter is of dimension d , generated from the Laplace approximation (Tierney & Kadane, 1986). Finally, for both UNI and Hilbert-OMP, we use NUTS to draw samples from the coresset posterior approximation.

4.1. Synthetic Gaussian

We first demonstrate the performance of SHF on a synthetic Gaussian-location model,

$$\theta \sim \mathcal{N}(0, I) \quad \text{and} \quad \forall n \in [N], \quad X_n \stackrel{\text{i.i.d.}}{\sim} \mathcal{N}(\theta, cI),$$

where $\theta, X_n \in \mathbb{R}^d$. We set $c = 100$, $d = 10$, $N = 10000$. This model has a closed form posterior distribution $\pi = \mathcal{N}\left(\frac{\sum_{n=1}^N X_n}{c+N}, \frac{c}{c+N}I\right)$. The data are generated from the distribution $X_n \stackrel{\text{i.i.d.}}{\sim} \mathcal{N}(10, cI)$. More details may be found in Appendix A.1.

Fig. 2a compares the ELBO values of SHF, HIS, and UHA across all optimization iterations. From this figure, we can see that SHF and UHA-Full result in the highest ELBO, and hence tightest bound on the log normalization constant of the target. In this problem, since we have access to the exact posterior distribution in closed form, we can also estimate the θ -marginal KL divergence directly, as shown in Fig. 2b. Here we see that the posterior approximation produced by SHF provides a significantly lower KL than the other competing methods. Figs. 2c and 2d demonstrate that this reduction in KL divergence is primarily due to a lower relative error in the approximate posterior mean provided by SHF, with a roughly equally accurate approximate posterior covariance as in UHA-Full.

Fig. 3a shows the time required for each method to evaluate

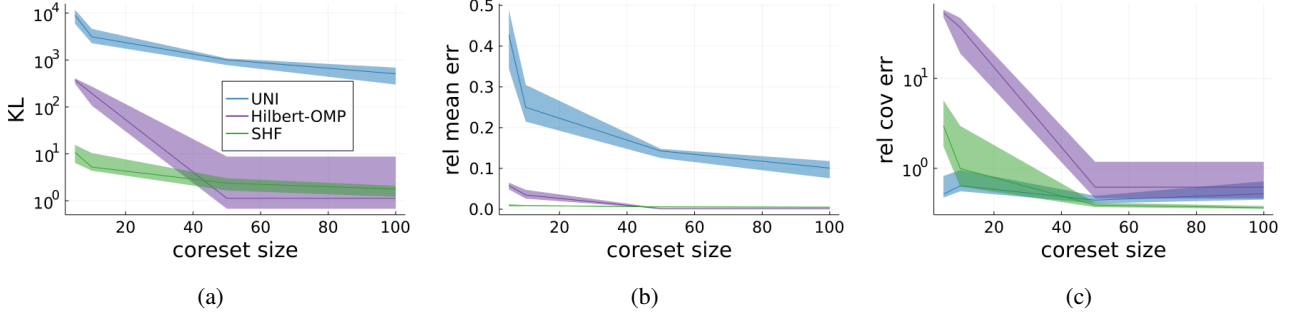


Figure 4. Synthetic Gaussian coresets comparison: estimated KL divergence (Fig. 4a), relative 2-norm mean error (Fig. 4b), and relative Frobenius norm covariance error (Fig. 4c) versus coresets size.

the density of the joint distribution θ, ρ^4 , and Fig. 3b shows the time required for each method to generate samples. It is clear from both figures that the use of a coresets in SHF improves the sample generation and density evaluation time by more than an order of magnitude. Fig. 3c compares the training times of SHF, HIS-Coresets, and UHA-Coresets (recall that due to the use of subsampled minibatch flow dynamics during training, HIS-Full and UHA-Full share the same training time as their -Coresets versions). The relative speeds of training generally match those of generating a sample from the target posteriors.

Finally, Fig. 4 compares the quality of coresets constructed via SHF, uniform subsampling (UNI), and Hilbert coresets with orthogonal matching pursuit (Hilbert-OMP). Note that in this problem, the Laplace approximation is exact (the true posterior is Gaussian), and hence Hilbert-OMP constructs a coresets using samples from the true posterior. Despite this, SHF provides coresets of comparable quality, in addition to enabling tractable i.i.d. sampling, density evaluation, normalization constant bounds, and straightforward construction via stochastic optimization.

4.2. Bayesian Linear Regression

In the setting of Bayesian linear regression, we are given a set of data points $(x_n, y_n)_{n=1}^N$, each consisting of a feature $x_n \in \mathbb{R}^p$ and response $y_n \in \mathbb{R}$, and a model of the form

$$\begin{bmatrix} \beta \\ \log \sigma^2 \end{bmatrix} \sim \mathcal{N}(0, I)$$

$$\forall n \in [N], \quad y_n \mid x_n, \beta, \sigma^2 \stackrel{\text{indep}}{\sim} \mathcal{N}\left(\beta^T \begin{bmatrix} 1 \\ x_n \end{bmatrix}, \sigma^2\right)$$

where $\beta \in \mathbb{R}^{p+1}$ is a vector of regression coefficients and $\sigma^2 \in \mathbb{R}_+$ is the noise variance. The dataset⁵ that we use

⁴As mentioned in Section 2.4, UHA involves multiple auxiliary momentum variables introduced by stochastic refreshment. Hence for UHA we evaluate the joint density of all variables.

⁵This dataset consists of airport data from https://www.transtats.bts.gov/DL_SelectFields.asp?gnoyr_VQ=FGJ and weather data from <https://wunderground.com>.

consists of $N = 14,793$ flights, each containing $p = 10$ features (e.g., the distance of the flight, weather conditions, departure time, etc), and the response variable equal to the difference, in minutes, between the scheduled and actual departure times. More details can be found in Appendix A.2.

Since we no longer have the posterior distribution in closed form, we estimate the mean and covariance using 15,000 samples from Stan (Carpenter et al., 2017) and treat them as the true posterior mean and covariance. Figs. 5a to 5c show the marginal KL, relative mean error, and relative covariance error of SHF, HIS, and UHA, where the marginal KL is estimated using the Gaussian approximation of the posterior with the estimated mean and covariance. We see that SHF provides the highest quality posterior approximation. Furthermore, Fig. 5d shows that SHF provides a significant improvement in the marginal KL compared with competing coresset constructions UNI and Hilbert-OMP. This is due to the true posterior no longer being Gaussian; the Laplace approximation required by Hilbert-OMP fails to capture the shape of the posterior. Additional plots can be found in Appendix A.2.

4.3. Bayesian Logistic Regression

Given a set of data points $(x_n, y_n)_{n=1}^N$, where $x_n \in \mathbb{R}^p$ denotes the set of p features and $y_n \in \{0, 1\}$ denotes the corresponding label, we perform posterior inference in the Bayesian logistic regression model with a Cauchy prior

$$\forall i \in [p+1], \quad \theta_i \stackrel{\text{i.i.d.}}{\sim} \text{Cauchy}(0, 1)$$

$$\forall n \in [N], \quad y_n \stackrel{\text{indep}}{\sim} \text{Bern}\left(\frac{1}{1 + \exp(-\theta^T \begin{bmatrix} 1 \\ x_n \end{bmatrix})}\right),$$

where $\theta \in \mathbb{R}^{p+1}$. We use the same dataset as in the previous example, but in this case the labels indicate whether each flight is cancelled. Of the flights in the dataset, roughly 10%

and weather data from <https://wunderground.com>.

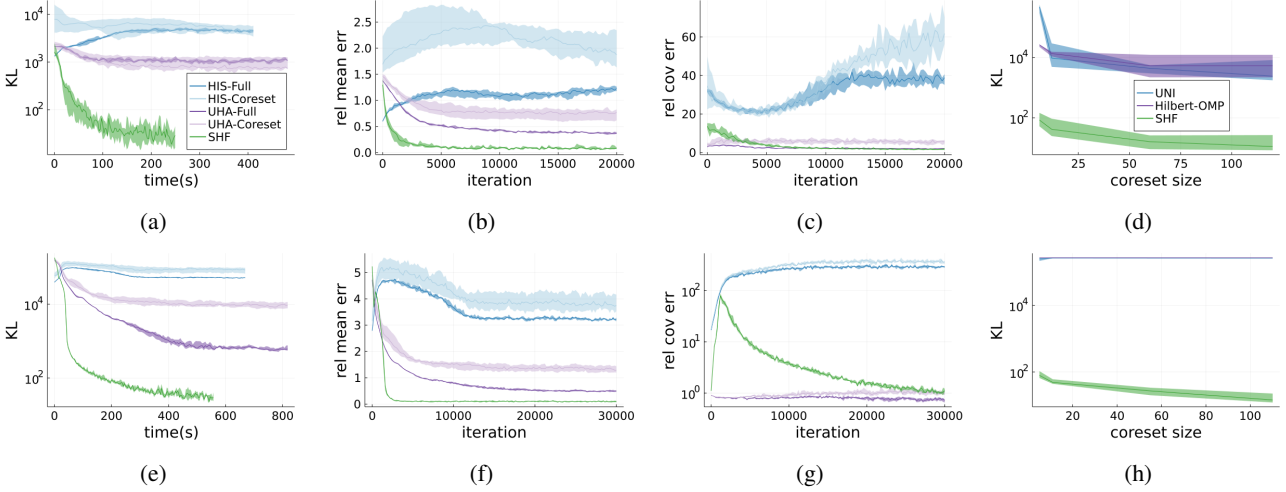


Figure 5. Linear regression (top row) and logistic regression (bottom row) results: estimated KL divergence versus training time (Figs. 5a and 5e), relative 2-norm mean error (Figs. 5b and 5f), relative Frobenius norm covariance error (Figs. 5c and 5g), and estimated KL divergence versus coresset size (Figs. 5d and 5h).

were cancelled. More details can be found in Appendix A.3.

As in the Bayesian linear regression example, we use 15,000 samples from Stan to estimate the true posterior mean and covariance, which are then used to fit a Gaussian approximation to estimate the marginal KL. To account for the class imbalance problem present in the dataset, we stratify the data when subsampling to construct the coresset for SHF with half the data having label 1 and the other half with label 0. The results in Figs. 5e to 5h are similar to those from the Bayesian linear regression example; SHF provides high quality variational approximations to the posterior. Additional plots can be found in Appendix A.3.

5. Conclusion

This paper introduced sparse Hamiltonian flows, a novel coresset construction method that enables tractable i.i.d. sampling, density evaluation, and marginal evidence lower bounds. The method first randomly selects a small subset of data, and then constructs a flow from sparse Hamiltonian dynamics using only those weighted potential functions in the subsample. Novel momentum quasi-refreshment steps provide the flow with the flexibility to match target Bayesian posteriors without introducing additional auxiliary variables. Theoretical results show that, in a representative model, the method is able to create an exact coresset posterior while compressing the dataset to a logarithm of its original size, and that the quasi-refreshment steps are guaranteed to reduce the KL divergence to the target. Experiments demonstrate that the method provides high quality coresset posterior approximations. Future work includes developing a wider variety of general-purpose quasi-refreshment moves.

Acknowledgements

All authors were supported by a National Sciences and Engineering Research Council of Canada (NSERC) Discovery Grant, NSERC Discovery Launch Supplement, and a gift from Google LLC.

References

- Agarwal, P., Har-Peled, S., and Varadarajan, K. Geometric approximation via coresets. *Combinatorial and Computational Geometry*, 52:1–30, 2005.
- Ahn, S., Korattikara, A., and Welling, M. Bayesian posterior sampling via stochastic gradient Fisher scoring. In *International Conference on Machine Learning*, 2012.
- Bardenet, R., Doucet, A., and Holmes, C. On Markov chain Monte Carlo methods for tall data. *Journal of Machine Learning Research*, 18:1–43, 2017.
- Baydin, A. G., Pearlmutter, B., Radul, A., and Siskind, J. Automatic differentiation in machine learning: a survey. *Journal of Machine Learning Research*, 18:1–43, 2018.
- Betancourt, M. The fundamental incompatibility of Hamiltonian Monte Carlo and data subsampling. In *International Conference on Machine Learning*, 2015.
- Böröczky, K. and Wintsche, G. Covering the sphere by equal spherical balls. In Aronov, B., Basu, S., Pach, J., and Sharir, M. (eds.), *Discrete and Computational Geometry*, volume 25 of *Algorithms and Combinatorics*, pp. 235–251. Springer, 2003.

Bottou, L. Stochastic Learning. In Bousquet, O., von Luxburg, U., and Rätsch, G. (eds.), *Advanced Lectures on Machine Learning: ML Summer Schools 2003*, pp. 146–168. Springer Berlin Heidelberg, 2004.

Campbell, T. and Beronov, B. Sparse variational inference: Bayesian coresets from scratch. In *Advances in Neural Information Processing Systems*, 2019.

Campbell, T. and Broderick, T. Bayesian coreset construction via greedy iterative geodesic ascent. In *International Conference on Machine Learning*, 2018.

Campbell, T. and Broderick, T. Automated scalable Bayesian inference via Hilbert coresets. *Journal of Machine Learning Research*, 20(15), 2019.

Carpenter, B., Gelman, A., Hoffman, M., Lee, D., Goodrich, B., Betancourt, M., Brubaker, M., Guo, J., Li, P., and Riddell, A. Stan: A probabilistic programming language. *Journal of Statistical Software*, 76(1), 2017.

Caterini, A., Doucet, A., and Sejdinovic, D. Hamiltonian variational auto-encoder. In *Advances in Neural Information Processing Systems*, 2018.

Feldman, D. and Langberg, M. A unified framework for approximating and clustering data. In *Symposium on Theory of Computing*, 2011.

Feldman, D., Faulkner, M., and Krause, A. Scalable training of mixture models via coresets. In *Advances in Neural Information Processing Systems*, 2011.

Feldman, D., Schmidt, M., and Sohler, C. Turning big data into tiny data: constant-size coresets for k -means, PCA, and projective clustering. In *Symposium on Discrete Algorithms*, 2013.

Geffner, T. and Domke, J. MCMC variational inference via uncorrected Hamiltonian annealing. In *Advances in Neural Information Processing Systems*, 2021.

Gelman, A., Carlin, J., Stern, H., Dunson, D., Vehtari, A., and Rubin, D. *Bayesian data analysis*. CRC Press, 3rd edition, 2013.

Habib, R. and Barber, D. Auxiliary variational MCMC. In *International Conference on Learning Representations*, 2018.

Hoffman, M. and Gelman, A. The No-U-Turn Sampler: adaptively setting path lengths in Hamiltonian Monte Carlo. *Journal of Machine Learning Research*, 15(1): 1593–1623, 2014.

Hoffmann, M., Blei, D., Wang, C., and Paisley, J. Stochastic variational inference. *Journal of Machine Learning Research*, 14:1303–1347, 2013.

Huggins, J., Campbell, T., and Broderick, T. Coresets for scalable Bayesian logistic regression. In *Advances in Neural Information Processing Systems*, 2016.

Jankowiak, M. and Phan, D. Surrogate likelihoods for variational annealed importance sampling. *arXiv:2112.12194*, 2021.

Johnsdrow, J., Pillai, N., and Smith, A. No free lunch for approximate MCMC. *arXiv:2010.12514*, 2020.

Jordan, M., Ghahramani, Z., Jaakkola, T., and Saul, L. An introduction to variational methods for graphical models. *Machine Learning*, 37:183–233, 1999.

Kingma, D. and Ba, J. Adam: A method for stochastic optimization. *International Conference on Learning Representations*, 2014.

Korattikara, A., Chen, Y., and Welling, M. Austerity in MCMC land: cutting the Metropolis-Hastings budget. In *International Conference on Machine Learning*, 2014.

Kucukelbir, A., Tran, D., Ranganath, R., Gelman, A., and Blei, D. Automatic Differentiation Variational Inference. *Journal of Machine Learning Research*, 18(14), 2017.

Maclaurin, D. and Adams, R. Firefly Monte Carlo: exact MCMC with subsets of data. In *Conference on Uncertainty in Artificial Intelligence*, 2014.

Manousakis, D., Xu, Z., Mascolo, C., and Campbell, T. Bayesian pseudocoresets. In *Advances in Neural Information Processing Systems*, 2020.

Nagapetyan, T., Duncan, A., Hasenclever, L., Vollmer, S., Szpruch, L., and Zygalakis, K. The true cost of stochastic gradient Langevin dynamics. *arXiv:1706.02692*, 2017.

Neal, R. *Bayesian Learning for Neural Networks*. Lecture Notes in Statistics, No. 118. Springer-Verlag, 1996.

Neal, R. Hamiltonian importance sampling. Banff International Research Station (BIRS) Workshop on Mathematical Issues in Molecular Dynamics, 2005.

Neal, R. MCMC using Hamiltonian dynamics. In Brooks, S., Gelman, A., Jones, G., and Meng, X.-L. (eds.), *Handbook of Markov chain Monte Carlo*, chapter 5. CRC Press, 2011.

Pati, Y. C., Rezaifar, R., and Krishnaprasad, P. S. Orthogonal matching pursuit: Recursive function approximation with applications to wavelet decomposition. In *Proceedings of 27th Asilomar Conference on Signals, Systems and Computers*, pp. 40–44. IEEE, 1993.

Quiroz, M., Kohn, R., and Dang, K.-D. Subsampling MCMC—an introduction for the survey statistician. *Sankhya: The Indian Journal of Statistics*, 80-A:S33–S69, 2018.

Quiroz, M., Kohn, R., Villani, M., and Tran, M.-N. Speeding up MCMC by efficient data subsampling. *Journal of the American Statistical Association*, 114(526):831–843, 2019.

Ranganath, R., Gerrish, S., and Blei, D. Black box variational inference. In *International Conference on Artificial Intelligence and Statistics*, 2014.

Rezende, D. and Mohamed, S. Variational inference with normalizing flows. In *International Conference on Machine Learning*, 2015.

Robbins, H. and Monro, S. A stochastic approximation method. *The Annals of Mathematical Statistics*, pp. 400–407, 1951.

Robert, C. and Casella, G. *Monte Carlo Statistical Methods*. Springer, 2nd edition, 2004.

Robert, C. and Casella, G. A short history of Markov Chain Monte Carlo: subjective recollections from incomplete data. *Statistical Science*, 26(1):102–115, 2011.

Salimans, T., Kingma, D., and Welling, M. Markov chain Monte Carlo and variational inference: bridging the gap. In *International Conference on Machine Learning*, 2015.

Thin, A., Kotelevskii, N., Doucet, A., Durmus, A., Moulines, E., and Panov, M. Monte Carlo variational auto-encoders. In *International Conference on Machine Learning*, 2021.

Tierney, L. and Kadane, J. Accurate approximations for posterior moments and marginal densities. *Journal of the American Statistical Association*, 81(393):82–86, 1986.

Wainwright, M. and Jordan, M. Graphical models, exponential families, and variational inference. *Foundations and Trends in Machine Learning*, 1(1–2):1–305, 2008.

Welling, M. and Teh, Y. W. Bayesian learning via stochastic gradient Langevin dynamics. In *International Conference on Machine Learning*, 2011.

Wolf, C., Karl, M., and van der Smagt, P. Variational inference with Hamiltonian Monte Carlo. *arXiv:1609.08203*, 2016.

Zhang, G., Hsu, K., Li, J., Finn, C., and Grosse, R. Differentiable annealed importance sampling and the perils of gradient noise. In *Advances in Neural Information Processing Systems*, 2021a.

Zhang, J., Khanna, R., Kyrillidis, A., and Koyejo, O. Bayesian coresets: revisiting the nonconvex optimization perspective. In *Artificial Intelligence in Statistics*, 2021b.

A. Details of experiments

We begin with general details that apply across all three experiments in the main text. For all three methods (SHF, HIS, and UHA), the unnormalized log target density used in computing the ELBO objective is estimated using a minibatch of $S = 100$ data points for each optimization iteration. For both HIS and UHA, the leapfrog transitions themselves are also based on a fresh uniformly sampled minibatch of size 30—the same as the coresnet size for SHF—at each optimization iteration. HIS and UHA both also involve tempering procedures, requiring optimization over the tempering schedule $0 \leq \beta_1 \leq \dots \leq \beta_{R-1} \leq \beta_R = 1$, where R denotes the number of tempering steps (equal to the number of quasi-refreshment / refreshment steps in all methods). We consider a reparameterization of $(\beta_1, \dots, \beta_R)$ to $(\alpha_1, \dots, \alpha_{R-1})$, where $\alpha_r = \text{Logit}(\beta_{r+1}/\beta_r)$ for $r \in \{1, \dots, R-1\}$, ensuring a set of unconstrained parameters. The initial value for each r is set to $\alpha_r = 1$. For UHA, the initial damping coefficient of its partial momentum refreshment is set to 0.5. We train all methods with ADAM with initial learning rate 0.001.

A.1. Synthetic Gaussian

To train SHF, a total of 5 quasi-refreshments are used with 10 leapfrog steps in between; a similar schedule is used in HIS and UHA for momentum tempering and refreshment respectively. The initial distribution is set to $\theta_0 \sim \mathcal{N}(0, I)$ and $\rho_0 \sim \mathcal{N}(0, I)$. For all methods, the number of optimization iterations is set to 20,000, and the initial leapfrog step size is set to 0.01 across all d dimensions.

A.2. Linear regression

To train SHF, a total of 8 quasi-refreshments are used with 10 leapfrog steps in between; a similar schedule is used in HIS and UHA for momentum tempering and refreshment respectively. The initial distribution is set to $\theta_0 \sim \mathcal{N}(10, 0.1I)$ and $\rho_0 \sim \mathcal{N}(0, I)$. For all methods, the number of optimization iterations is set to 20,000, and the initial leapfrog step size is set to 0.02 across all d dimensions. Figs. 6 and 7 provide additional results for this experiment. Fig. 6a shows that the ELBO obtained from SHF is a tighter lower bound of the log normalization constant compared to HIS and UHA. Fig. 6b shows that SHF produces a posterior mean closer to the target than that obtained by UNI or Hilbert-OMP. Although Fig. 6c shows that the relative covariance error of SHF is slightly larger, we note that this error keeps decreasing as we increase the coresnet size. Finally, Figs. 7a and 7b show the computational gain of using SHF to approximate density and generate posterior samples as compared to HIS and UHA.

A.3. Logistic regression

To train SHF, a total of 8 quasi-refreshments are used with 10 leapfrog steps in between; a similar schedule is used in HIS and UHA for momentum tempering and refreshment respectively. The initial distribution is set to $\theta_0 \sim \mathcal{N}(5, 10^{-3}I)$ and $\rho_0 \sim \mathcal{N}(0, I)$. For all methods, the number of optimization iterations is set to 30,000, and the initial leapfrog step size is set to 0.02 across all d dimensions. Figs. 6 and 7 provide additional results for this experiment; in particular, Figs. 6d to 6f, 7c and 7d contain results with similar conclusions as in the linear regression experiment.

B. Gaussian KL upper bound proof

Proof of Proposition 3.1. Suppose we are given a particular choice $\mathcal{I} \subseteq [N]$ of N indices of size $|\mathcal{I}| = M \in \mathbb{N}$, $M \leq N$. Let $\mathcal{W}_{\mathcal{I}} = \{w \in \mathbb{R}_+^N : \forall n \in [N], n \notin \mathcal{I} \implies w_n = 0\}$. In the d -dimensional normal location model, the exact and $w \in \mathcal{W}_{\mathcal{I}}$ -coresnet posteriors are multivariate Gaussian distributions, denoted as $\mathcal{N}(\mu_1, \Sigma_1)$ and $\mathcal{N}(\mu_w, \Sigma_w)$ respectively, with mean and covariance

$$\Sigma_1 = \frac{1}{1+N} I, \quad \mu_1 = \Sigma_1 \left(\sum_{n=1}^N X_n \right) \quad \text{and} \quad \Sigma_w = \frac{I}{1 + (\sum_{n \in \mathcal{I}} w_n)}, \quad \mu_w = \Sigma_w \left(\sum_{n \in \mathcal{I}} w_n X_n \right).$$

The KL divergence between these two distributions is

$$D_{\text{KL}}(\pi_w \parallel \pi) = \frac{1}{2} \left[-d \log \left(\frac{1+N}{1 + \sum_{n \in \mathcal{I}} w_n} \right) - d + d \left(\frac{1+N}{1 + \sum_{n \in \mathcal{I}} w_n} \right) + (\mu_1 - \mu_w)^T \Sigma_1^{-1} (\mu_1 - \mu_w) \right].$$

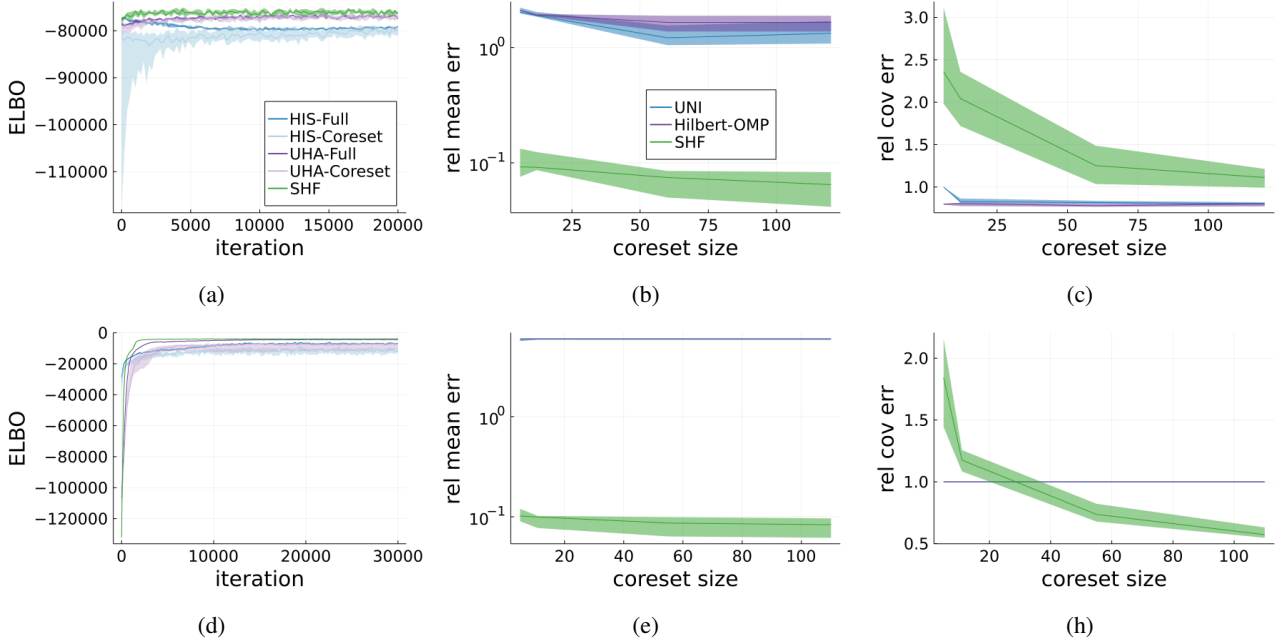


Figure 6. Linear (top row, Figs. 6a to 6c) and logistic (bottom row Figs. 6d to 6f) regression: posterior approximation quality results.

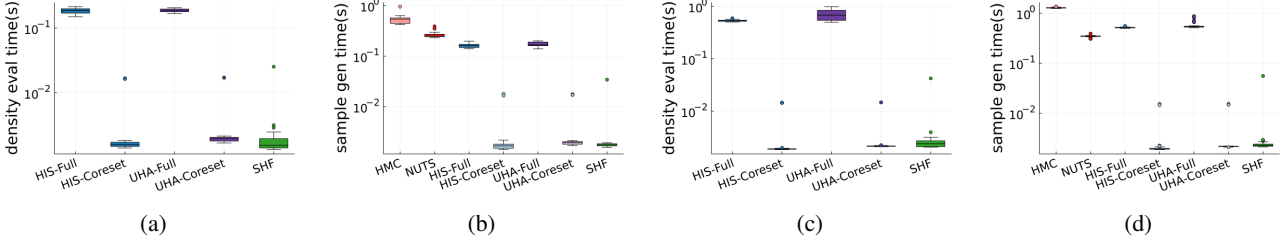


Figure 7. Linear (Figs. 7a and 7b) and logistic (Figs. 7c and 7d) regression: timing results.

We can bound this quantity above by adding the constraint $\sum_{n \in \mathcal{I}} w_n = N$, yielding

$$\min_{w \in \mathcal{W}_{\mathcal{I}}} D_{KL}(\pi_w || \pi) \leq \min_{w \in \Delta^{M-1}} \frac{N^2}{2(N+1)} \left\| \bar{X} - \sum_{n \in \mathcal{I}} w_n X_n \right\|^2,$$

where $\bar{X} = \frac{1}{N} \sum_{n=1}^N X_n$, and Δ^{M-1} is the $M-1$ -dimensional simplex $w \geq 0, 1^T w = 1$. We aim to show that with high probability (over uniform random choice of \mathcal{I} and realizations of $X_n, n \in [N]$), there exists a $w \in \Delta^{M-1}$ such that $\bar{X} = \sum_{n \in \mathcal{I}} w_n X_n$, and hence the optimal KL divergence is 0.

Since $X_n \stackrel{\text{i.i.d.}}{\sim} \mathcal{N}(0, I)$, $\sqrt{N} \bar{X} \sim \mathcal{N}(0, I)$, so $\|\sqrt{N} \bar{X}\|^2 \sim \chi^2(d)$ and therefore for any $s > \sqrt{d/N}$,

$$\mathbb{P}(\|\bar{X}\| > s) \leq \left(\frac{s^2 N}{d} e^{1 - \frac{s^2 N}{d}} \right)^{d/2}. \quad (10)$$

In other words, as N increases, we can expect \bar{X} to concentrate around the origin. Therefore as long as the convex hull of $X_n, n \in \mathcal{I}$ contains a ball of some fixed radius around the origin with high probability, we know that \bar{X} is a convex combination of $X_n, n \in \mathcal{I}$. The radius of the largest origin-centered ball inside the convex hull of $X_n, n \in \mathcal{I}$ can be expressed as

$$r^* = \min_{a \in \mathbb{R}^d: \|a\|=1, b \geq 0} b \quad \text{s.t.} \quad \forall n \in \mathcal{I}, \quad a^T X_n - b \leq 0 = \min_{a \in \mathbb{R}^d: \|a\|=1} \max_{n \in \mathcal{I}} a^T X_n.$$

By Böröczky & Wintsche (2003, Corollary 1.2), S^d can be covered by

$$N_d(\phi) = \frac{C \cdot \cos \phi}{\sin^d \phi} d^{\frac{3}{2}} \log(1 + d \cos^2 \phi) \leq \phi^{-d} A_d, \quad A_d = C e^{\frac{d}{2}} d^{\frac{3}{2}} \log(1 + d). \quad (11)$$

balls of radius $0 < \phi \leq \arccos \frac{1}{\sqrt{d+1}}$, where C is a universal constant. Denote the centres of these balls $a_i \in S^d$, $i = 1, \dots, N_d(\phi)$. Then

$$\begin{aligned} r^* &\geq \min_{i \in [N_d(\phi)], v \in \mathbb{R}^d: \|v\| \leq \phi} \max_{n \in \mathcal{I}} (a_i + v)^T X_n \\ &\geq \min_{i \in [N_d(\phi)]} \max_{n \in \mathcal{I}} a_i^T X_n - \phi \|X_n\|. \end{aligned}$$

Therefore the probability that the largest origin-centred ball enclosed in the convex hull is small is bounded above by

$$\begin{aligned} \mathbb{P}(r^* \leq t) &\leq \mathbb{P}\left(\min_{i \in [N_d(\phi)]} \max_{n \in \mathcal{I}} a_i^T X_n - \phi \|X_n\| \leq t\right) \\ &\leq N_d(\phi) \mathbb{P}\left(\max_{n \in \mathcal{I}} a_i^T X_n - \phi \|X_n\| \leq t\right) \\ &= N_d(\phi) \mathbb{P}(a^T Z - \phi \|Z\| \leq t)^M, \end{aligned}$$

for $a \in S^d$ and $Z \sim \mathcal{N}(0, I)$. Since Z has a spherically symmetric distribution, a is arbitrary, so we can choose $a = (1 \ 0 \ \dots \ 0)^T$. If we let $U \sim \mathcal{N}(0, 1)$ and $V \sim \chi^2(d-1)$ be independent, this yields

$$\begin{aligned} \mathbb{P}(a^T Z - \phi \|Z\| \leq t) &= \mathbb{P}(U - \phi \sqrt{U^2 + V} \leq t) \\ &= \mathbb{P}(U - t \leq \phi \sqrt{U^2 + V}) \\ &\leq \mathbb{P}(U < 2t) + \mathbb{P}(V \geq \phi^{-2}(U - t)^2 - U^2, U \geq 2t) \\ &\leq \Phi(2t) + \mathbb{P}(V' \geq \phi^{-2}t^2), \end{aligned}$$

where $V' \sim \chi^2(d)$ and $\Phi(\cdot)$ is the CDF of the standard normal. Therefore as long as $t > \phi \sqrt{d}$,

$$\begin{aligned} \mathbb{P}(V' \geq \phi^{-2}t^2) &= \mathbb{P}\left(V' \geq d \left(\frac{t}{\phi \sqrt{d}}\right)^2\right) \\ &\leq \left(\left(\frac{t}{\phi \sqrt{d}}\right)^2 e^{1 - \left(\frac{t}{\phi \sqrt{d}}\right)^2}\right)^{d/2}. \end{aligned}$$

We now combine the above results to show that for any $t > \phi \sqrt{d}$,

$$\mathbb{P}(r^* \leq t) \leq N_d(\phi) \left(\Phi(2t) + d^{-\frac{d}{2}} e^{\frac{d}{2}} \phi^{-d} t^d e^{-\frac{1}{2}\phi^{-2}t^2}\right)^M. \quad (12)$$

Finally we combine the bound on the norm of \bar{X} Eq. (10), the bound on r^* Eq. (12), and the covering number of S^d Eq. (11) for the final result. For any $t > \max\{\phi \sqrt{d}, \sqrt{d/N}\}$ and $\phi \leq \arccos \frac{1}{\sqrt{d+1}}$,

$$\mathbb{P}(\bar{X} \notin \text{conv}(X_n)_{n \in \mathcal{I}}) \leq d^{-\frac{d}{2}} e^{\frac{d}{2}} t^d N^{d/2} e^{-\frac{1}{2}t^2 N} + \phi^{-d} A_d \left(\Phi(2t) + d^{-\frac{d}{2}} e^{\frac{d}{2}} \phi^{-d} t^d e^{-\frac{1}{2}\phi^{-2}t^2}\right)^M$$

Set $\phi = \sqrt{\frac{1}{N}}$ and $t = s \sqrt{d/N}$. As long as $N \geq 2$ and $s > 1$, we are guaranteed that $t > \max\{\phi \sqrt{d}, \sqrt{d/N}\}$ and $\phi \leq \arccos \frac{1}{\sqrt{d+1}}$ as required, and so

$$\mathbb{P}(\bar{X} \notin \text{conv}(X_n)_{n \in \mathcal{I}}) \leq e^{\frac{d}{2}} s^d e^{-\frac{d}{2}s^2} + N^{\frac{d}{2}} A_d \left(\Phi\left(s \sqrt{\frac{4d}{N}}\right) + e^{\frac{d}{2}} s^d e^{-\frac{d}{2}s^2}\right)^M.$$

If we set $s = \sqrt{\log N + 1}$,

$$e^{\frac{d}{2}} s^d e^{-\frac{d}{2}s^2} = N^{-\frac{d}{2}} (\log N + 1)^{\frac{d}{2}} \quad \Phi\left(s\sqrt{\frac{4d}{N}}\right) = \frac{1}{2} + O\left(\sqrt{\frac{\log N}{N}}\right).$$

So then setting $M = d \log_2(N) - \frac{d}{2} \log_2(\log(N)) + \log_2 A_d$ yields the claimed result. \square

C. Gaussian KL lower bound proof

Proof of Proposition 3.2. Let $z(t) = (\theta_t, \rho_t)$. The evolution of $z(t)$ is determined by a time-inhomogeneous linear ordinary differential equation,

$$\frac{dz(t)}{dt} = A(t)z(t) \quad A(t) = \begin{pmatrix} 0 & 1 \\ -\sigma^{-2} & -\gamma(t) \end{pmatrix},$$

with solution

$$z(t) = e^{B(t)}z(0) \quad B(t) = \begin{pmatrix} 0 & t \\ -\sigma^{-2}t & g(t) \end{pmatrix}, \quad g(t) = -\int_0^t \gamma(t)dt.$$

Therefore by writing $\bar{\pi}_0 = \mathcal{N}(m(0), \Sigma(0))$, $z(t) \sim q_t = \mathcal{N}(m(t), \Sigma(t))$, where

$$m(t) = e^{B(t)}m(0) \quad \Sigma(t) = e^{B(t)}\Sigma(0)e^{B(t)^T}. \quad (13)$$

The second result follows because tempered Hamiltonian dynamics where $\gamma(t) = 0$ identically is just standard Hamiltonian dynamics. For the first result, suppose $q_0 = \mathcal{N}\left(\begin{pmatrix} \mu \\ 0 \end{pmatrix}, \begin{pmatrix} 1 & 0 \\ 0 & \beta^2 \end{pmatrix}\right)$ for some $\mu \in \mathbb{R}, \beta \in \mathbb{R}_+$. Note that in this case, it suffices to consider

$$m(0) = \begin{pmatrix} \mu \\ 0 \end{pmatrix} \quad \Sigma(0) = I. \quad (14)$$

This is because the function $\gamma(t)$ is arbitrary; one can, for example, set $\gamma(t) = -\epsilon^{-1} \log \beta$ for $t \in [0, \epsilon]$ for an arbitrarily small $\epsilon > 0$, such that the state at time ϵ is arbitrarily close to the desired initial condition. The KL divergence from q_t to $\bar{\pi}$ is

$$\begin{aligned} D_{\text{KL}}(q_t || \bar{\pi}) &= \frac{1}{2} \left[\log \left(\frac{\det \Sigma}{\det \Sigma(t)} \right) - 2 + \text{tr}(\Sigma^{-1} \Sigma(t)) + m(t)^T \Sigma^{-1} m(t) \right] \\ &= \frac{1}{2} \left[\log \left(\frac{\det \Sigma}{\det \Sigma(t)} \right) - 2 + \text{tr}(\Sigma^{-1} (\Sigma(t) + m(t)m(t)^T)) \right]. \end{aligned}$$

By Eqs. (13) and (14) and the identity $\text{tr } A^T A = \|A\|_F^2$,

$$\begin{aligned} D_{\text{KL}}(q_t || \bar{\pi}) &= \frac{1}{2} \left[\log \left(\frac{\det \Sigma}{\det \Sigma(t)} \right) - 2 + \text{tr}(\Sigma^{-1} e^{B(t)} (I + m(0)m(0)^T) e^{B(t)^T}) \right] \\ &= \frac{1}{2} \left[\log \left(\frac{\det \Sigma}{\det \Sigma(t)} \right) - 2 + \left\| \Sigma^{-\frac{1}{2}} e^{B(t)} (I + m(0)m(0)^T)^{\frac{1}{2}} \right\|_F^2 \right]. \end{aligned} \quad (15)$$

From this point onward we will drop the explicit dependence on t for notational brevity. Note that B has eigendecomposition $B = VDV^{-1}$ where

$$\begin{aligned} h &= \frac{g}{2t\sigma^{-1}} \quad \lambda_+ = h + \sqrt{h^2 - 1} \quad \lambda_- = h - \sqrt{h^2 - 1} \\ V &= t \begin{pmatrix} 1 & 0 \\ 0 & \sigma^{-1} \end{pmatrix} \begin{pmatrix} 1 & 1 \\ \lambda_+ & \lambda_- \end{pmatrix} \quad D = t\sigma^{-1} \begin{pmatrix} \lambda_+ & 0 \\ 0 & \lambda_- \end{pmatrix}. \end{aligned}$$

Also note that if $|h| < 1$, this decomposition has complex entries, but e^B is always a real matrix.

Then the log-determinant term in Eq. (15) can be written as

$$\log \left(\frac{\det \Sigma}{\det \Sigma(t)} \right) = \log \frac{\det \Sigma}{\det \Sigma(0) \det e^{2D}} = \log \frac{\sigma^2}{e^{2g}} = \log \frac{\sigma^2}{e^{4ht\sigma^{-1}}} = 2(\log \sigma - 2ht\sigma^{-1}). \quad (16)$$

By $e^B = V e^D V^{-1}$, the squared Frobenius norm term in Eq. (15) is

$$\begin{aligned} \|\cdot\|_F^2 &:= \left\| \Sigma^{-\frac{1}{2}} e^{B(t)} (I + m(0)m(0)^T)^{\frac{1}{2}} \right\|_F^2 \\ &= \frac{\sigma^{-2} (e_+ - e_-)^2}{(\lambda_- - \lambda_+)^2} \left((1 + \mu^2) + \sigma^2 + (1 + \mu^2) \left(\frac{\lambda_- e_+ - \lambda_+ e_-}{e_+ - e_-} \right)^2 + \sigma^2 \left(\frac{\lambda_- e_- - \lambda_+ e_+}{e_+ - e_-} \right)^2 \right). \end{aligned}$$

where $e_+ = e^{t\sigma^{-1}\lambda_+}$, $e_- = e^{t\sigma^{-1}\lambda_-}$. Let

$$\sinh(t, h) = \sinh(t\sigma^{-1}\sqrt{h^2 - 1}) \quad \cosh(t, h) = \cosh(t\sigma^{-1}\sqrt{h^2 - 1}),$$

we further simplify and get

$$\begin{aligned} \|\cdot\|_F^2 &= \frac{e^{2th\sigma^{-1}}}{\sigma^2} \left(\frac{\sinh(t, h)^2}{h^2 - 1} (1 + \mu^2 + \sigma^2) + (1 + \mu^2) \left(\frac{h \sinh(t, h)}{\sqrt{h^2 - 1}} - \cosh(t, h) \right)^2 + \right. \\ &\quad \left. \sigma^2 \left(\frac{h \sinh(t, h)}{\sqrt{h^2 - 1}} + \cosh(t, h) \right)^2 \right). \end{aligned} \quad (17)$$

Define $a = t\sigma^{-1}\sqrt{h^2 - 1}$ and $b = \frac{h}{\sqrt{h^2 - 1}}$ for $h \neq 1$. Then together with Eqs. (16) and (17), Eq. (15) can be written as

$$\begin{aligned} D_{\text{KL}}(q_t || \bar{\pi}) &= \log \sigma - 2ab - 1 + \\ &\frac{e^{2ab}}{2\sigma^2} \left((b^2 - 1) \sinh(a)^2 (1 + \mu^2 + \sigma^2) + (1 + \mu^2) (b \sinh(a) - \cosh(a))^2 + \sigma^2 (b \sinh(a) + \cosh(a))^2 \right). \end{aligned} \quad (18)$$

Note that if $|h| > 1$, then $a \geq 0$ and $|b| > 1$; if $|h| < 1$, we can write $a = ia'$ for $a' \geq 0$ and $b = ib'$ for $b' \in (-\infty, -1) \cup (1, \infty)$. We now derive lower bounds for Eq. (18) over a and b under three cases: ($|h| > 1, b > 1$), ($|h| > 1, b < -1$), and ($|h| < 1$).

Case ($|h| > 1, b > 1$): Using the identity $\cosh(x)^2 - \sinh(x)^2 = 1$ and $\sinh(2x) = 2 \sinh(x) \cosh(x)$,

$$\begin{aligned} &\frac{e^{2ab}}{2\sigma^2} ((b^2 - 1) \sinh(a)^2 \sigma^2 + \sigma^2 (b \sinh(a) + \cosh(a))^2) \\ &= \frac{e^{2ab}}{2} ((b^2 - 1) \sinh(a)^2 + (b \sinh(a) + \cosh(a))^2) \\ &= \frac{e^{2ab}}{2} (2b^2 \sinh(a)^2 + 1 + b \sinh(2a)) \\ &\geq \frac{e^{2ab}}{2} + \frac{b \sinh(2a)}{2} \\ &\geq 2ab, \end{aligned}$$

where the second last line is obtained by noting that $2b^2 \sinh(a)^2 \geq 0$, $e^{2ab} \geq 2ab$, and the last line is obtained by noting that for $|h| > 1$ and $b > 1$, we have $\sinh(2a) \geq 2a$ and $e^{2ab} \geq 1$. Substituting this to Eq. (18),

$$\begin{aligned} D_{\text{KL}}(q_t || \bar{\pi}) &\geq \log \sigma - 1 + \frac{e^{2ab}}{2\sigma^2} ((b^2 - 1) \sinh(a)^2 (1 + \mu^2) + (1 + \mu^2) (b \sinh(a) - \cosh(a))^2) \\ &\geq \log \sigma - 1 + \frac{e^{2ab}(1 + \mu^2)}{2\sigma^2} (2b^2 \sinh(a)^2 + 1 - b \sinh(2a)). \end{aligned} \quad (19)$$

For $|h| > 1, b > 1$, we know $a \geq 0$. When $a \geq 0$ and $b > 1$,

$$\frac{\partial}{\partial a} \left(\log \sigma - 1 + \frac{e^{2ab}(1+\mu^2)}{2\sigma^2} (2b^2 \sinh(a)^2 + 1 - b \sinh(2a)) \right) \geq 0$$

and increases with a . Therefore

$$\arg \min_{a \in \mathbb{R}_+} \left(\log \sigma - 1 + \frac{e^{2ab}(1+\mu^2)}{2\sigma^2} (2b^2 \sinh(a)^2 + 1 - b \sinh(2a)) \right) = 0.$$

We also note that when we set $a = 0$, Eq. (19) is constant for all $b > 1$. Then by substituting $a = 0$ to Eq. (19), we get

$$D_{KL}(q_t || \bar{\pi}) \geq \log \sigma - 1 + \frac{(1+\mu^2)}{2\sigma^2} \geq \log \frac{1+\mu^2}{4\sigma}.$$

Case ($|h| > 1, b < -1$): Note in this case, $(b^2 - 1) \sinh(a)^2 \sigma^2 \geq 0$, $\sigma^2 (b \sinh(a) + \cosh(a))^2 \geq 0$, then we can lower bound Eq. (18) by

$$\begin{aligned} D_{KL}(q_t || \bar{\pi}) &\geq \log \sigma - 2ab - 1 + \frac{e^{2ab}}{2\sigma^2} \left((b^2 - 1) \sinh(a)^2 (1 + \mu^2) + (1 + \mu^2) (b \sinh(a) - \cosh(a))^2 \right) \\ &\geq \log \sigma - 2ab - 1 + \frac{e^{2ab}(1+\mu^2)}{2\sigma^2} (2b^2 \sinh(a)^2 + 1 - b \sinh(2a)) \\ &\geq \log \sigma - 2ab - 1 + \frac{e^{2ab}(1+\mu^2)}{2\sigma^2}, \end{aligned} \quad (20)$$

where the last line is obtained by noting $2b^2 \sinh(a)^2 - b \sinh(2a) \geq 0$ when $|h| > 1$ and $b < -1$. Also when $|h| > 1$ and $b < -1$, $ab \leq 0$. We then minimize Eq. (20) over $ab \leq 0$, treating ab as a single variable. The stationary point is at $(ab)^* = \frac{1}{2} \log \frac{2\sigma^2}{1+\mu^2}$. Since Eq. (20) is convex in ab , the optimum is at $(ab)^*$ if $\frac{2\sigma^2}{1+\mu^2} \leq 1$, and otherwise is at $(ab) = 0$. Therefore

$$\begin{aligned} D_{KL}(q_t || \bar{\pi}) &\geq \begin{cases} \log \sigma - 1 + \frac{1+\mu^2}{2\sigma^2} & \frac{2\sigma^2}{1+\mu^2} > 1 \\ \log \frac{1+\mu^2}{2\sigma} & \frac{2\sigma^2}{1+\mu^2} \leq 1 \end{cases} \\ &\geq \log \frac{1+\mu^2}{4\sigma}. \end{aligned}$$

Case ($|h| < 1$): Write $a = ia'$ and $b = ib'$ where $a' \geq 0$ and $b' \in (-\infty, -1) \cup (1, \infty)$. Using the identities $\sinh(x) = -i \sin(ix)$ and $\cosh(x) = \cos(ix)$, we can write Eq. (18) as

$$\begin{aligned} D_{KL}(q_t || \bar{\pi}) &= \log \sigma + 2a'b' - 1 + \\ &\frac{e^{-2a'b'}}{2\sigma^2} \left((b'^2 + 1) \sin(a)^2 (1 + \mu^2 + \sigma^2) + (1 + \mu^2) (b' \sin(a') + \cos(a'))^2 + \sigma^2 (b' \sin(a') - \cos(a'))^2 \right) \\ &= \log \sigma + 2a'b' - 1 + \frac{e^{-2a'b'}(1+\mu^2+\sigma^2)}{2\sigma^2} (b'^2 + 1 + b'f \sin(2a') - b'^2 \cos(2a')), \end{aligned}$$

where $f = \frac{1+\mu^2-\sigma^2}{1+\mu^2+\sigma^2}$. We know

$$a'^* = \arg \min_{a' \in \mathbb{R}_+} b'^2 + 1 + b'f \sin(2a') - b'^2 \cos(2a') = \frac{1}{2} \tan^{-1} \left(-\frac{f}{b'} \right) + n\pi,$$

where $n \in \mathbb{Z}$ such that $\frac{1}{2} \tan^{-1} \left(-\frac{f}{b'} \right) + n\pi \in \mathbb{R}_+$. Then by $\frac{e^{-2a'b'}(1+\mu^2+\sigma^2)}{2\sigma^2} \geq 0$,

$$\begin{aligned} D_{KL}(q_t || \bar{\pi}) &\geq \log \sigma + 2a'b' - 1 + \frac{e^{-2a'b'}(1+\mu^2+\sigma^2)}{2\sigma^2} (b'^2 + 1 + b'f \sin(2a'^*) - b'^2 \cos(2a'^*)) \\ &= \log \sigma + 2a'b' - 1 + \frac{e^{-2a'b'}(1+\mu^2+\sigma^2)}{2\sigma^2} (b'^2 + 1 - b'^2 \sqrt{1 + (f/b')^2}). \end{aligned}$$

Since $\sqrt{1+x} \leq 1 + \frac{1}{2}x$,

$$D_{KL}(q_t || \bar{\pi}) \geq \log \sigma + 2a'b' - 1 + \frac{e^{-2a'b'}(1 + \mu^2 + \sigma^2)}{2\sigma^2} \left(1 - \frac{1}{2}f^2\right). \quad (21)$$

The stationary point of Eq. (21) as a function in $a'b'$ is at

$$(a'b')^* = -\frac{1}{2} \log \frac{2\sigma^2}{(1 + \mu^2 + \sigma^2)(1 - \frac{1}{2}f^2)}.$$

Since Eq. (21) is convex in $a'b'$ and $a'b' \in \mathbb{R}$, we know the minimum of Eq. (21) is attained at $(a'b')^*$. Substituting $(a'b')^*$ back in Eq. (21) and noting $1 - \frac{1}{2}f^2 \geq \frac{1}{2}$, we get

$$\begin{aligned} D_{KL}(q_t || \bar{\pi}) &\geq \log \frac{(1 + \mu^2 + \sigma^2)(1 - \frac{1}{2}f^2)}{2\sigma} \\ &\geq \log \frac{1 + \mu^2 + \sigma^2}{4\sigma} \geq \log \frac{1 + \mu^2}{4\sigma}. \end{aligned}$$

□

D. Quasi-refreshment proofs

Proof of Proposition 3.3. Since R is a bijection,

$$D_{KL}(R(X), W || Y, Z) = D_{KL}(X, W || R^{-1}(Y), Z).$$

Because $Y \perp\!\!\!\perp Z$, and $R(X) \stackrel{d}{=} Y$,

$$\begin{aligned} D_{KL}(X, W || R^{-1}(Y), Z) &= D_{KL}(X || R^{-1}(Y)) + \mathbb{E}[D_{KL}((W|X) || Z)] \\ &= \mathbb{E}[D_{KL}((W|X) || Z)]. \end{aligned}$$

Then we add and subtract $D_{KL}(X || Y)$ to obtain the final result,

$$\mathbb{E}[D_{KL}((W|X) || Z)] = D_{KL}(X, W || Y, Z) - D_{KL}(X || Y).$$

□

Proof of Proposition 3.4. By assumption the distribution of Y given $Z = s$ is the same as that of $R_s(X)$ given $W = s$; so the result follows directly from the decomposition

$$\begin{aligned} D_{KL}(R_W(X), W || Y, Z) &= D_{KL}(W || Z) + \mathbb{E}[D_{KL}((R_S(X)|W = S) || (Y|Z = S))], \quad S \stackrel{d}{=} W \\ &= D_{KL}(W || Z). \end{aligned}$$

□